$W_{1-x}Mo_xO_3 \cdot 0.33H_2O$ Solid Solutions with Tunable Band Gap for Hydrogen Production

A. Arzola-Rubio[a], J. Camarillo-Cisneros[a], V. Collins-Martínez[a], L. De la Torre-Sáenz[a], F. Paraguay-Delgado[a*]

A Departamento de Materiales Nanoestructurados, Centro de Investigación en Materiales Avanzados S. C., CIMAV
Miguel de Cervantes 120, Chihuahua, Chih. México. CP 31109.
*Tel: +526144391107; e-mail: francisco.paraguay@cimav.edu.mx

ABSTRACT

A series of $W_{1-x}Mo_xO_3$ $0.33H_2O$ (x = 0, 0.25, 0.50, 0.75) nano/microstructures and MoO_3 $0.55H_2O$ microamorphous structures have been prepared by hydrothermal synthesis starting from aqueous Ammonium metatungstate hydrate ($(NH_4)_6H_2W_{12}O_{40}$ xH_2O) and Ammonium heptamolybdate tetrahydrate ($(NH_4)_6Mo_7O_{24}$ $4H_2O$) acidified solutions. The WO_3 $0.33H_2O$ crystal lattice can be substituted with up to 75% Mo without structural alterations of the orthorhombic host structure. With the increase of the Mo content (x) from 0 to 0.75, the band gap of the as-prepared $W_{1-x}Mo_xO_3$ $0.33H_2O$ nano/microstructures is narrowed from 2.62 to 2.10 eV. We employed first-principles calculations in the DFT and DFT+U framework as a meaning to confirm our experimental data and we obtained indirect semiconductors up to x=0.75. We suggest that the increasing Mo fraction (25, 50 and 75%), effects of the hydrothermal synthesis (pressure and temperature), hydrogen peroxide and pH are responsible for the narrowing of the band gap and increasing of the superficial area and presumably making hydrogen production feasible through the photocatalytic water splitting.

Keywords: H_2 production; water splitting; W/Mo solid solutions.

1. Introduction

Hydrogen is considered as an ideal energetic vector for the future. Hydrogen fuel can be produced from clean and renewable energy sources and, thus, its life cycle is clean and renewable. Solar and wind are the two major sources of renewable energy and they are also the promising sources for renewable hydrogen production. However, presently, renewable energy contributes only about 5% of the commercial hydrogen production primarily via water electrolysis, while other 95% hydrogen is mainly derived from fossil fuels [1]. Renewable hydrogen production is not popular yet because the cost is still high. Photovoltaic water electrolysis may become more competitive as the cost continues to decrease with the technology advancement; however, the considerable use of small band gap semiconducting materials may cause serious life cycle environmental impacts. Alternatively, photocatalytic water-splitting using unary and binary WO_3 compounds for hydrogen production offers a promising way for clean, low-cost and environmentally friendly production of hydrogen by solar energy. WO_3 compounds can be used for photocatalytic water splitting to produce hydrogen gas using visible solar light, because of its narrow bandgap. Earlier studies of the photo electrochemical behavior of both polycrystalline and monocrystalline WO_3 provided instructive knowledge for the development of photocatalytic water-splitting systems (Hodes et al. 1976; Hardee and Bard 1977). The difficulty in the overall water splitting (both reduction and oxidation of H_20 molecules are to be achieved) by WO3 is that the lower edge of the CB lies below the redox potential of H_20/H_2. This means that the reduction of water molecules to generate hydrogen gas is thermodynamically unfavorable (Gissler and Memming 1977). Applying a bias potential to the system can overcome the energy barrier for the photogenerated electrons to be ejected into the adsorbed water molecules (Santato et al. 2001). Coupling with other semiconductor materials (Abe et al. 2005) and doping by metal ions (Hwang et al. 2002; Hameed et al. 2004) are other alternatives to make use of the oxidation power of WO_3 for water splitting. WO_3 also found interesting applications in electrochromic (Papacfthimiou et al. 2001; Badilcscu and Ashrit 2003; Baeck et al. 2003) and photochromic (Shigesato 1991; Bechinger et al. 1996; Su et al. 1997; Xu et al. 2000; Kim et al. 2006) devices such as large area displays and "smart windows" because WO_3 films can be switched between different optical states under different electro-chemical or optical conditions. The electrochromic effect is caused by the electrochemical reaction between the WO_3 electrode and protons in the electrolyte solution, under the influence of a bias potential to provide charge carriers (electrons in this case). The electrons can then create color centers by reducing the W^{6+} species to W^{5+} species. The photochromism effect of WO_3 is due to the formation of an identical absorption band upon light irradiation (Bechinger et al. 1993). This process is completely reversible by exposing the reduced sample to oxygen gas. DFT has been a handy tool to corroborate gap experimental data and also as a method itself to use in simulate tendencies. Recently, Zhou et al. was capable of modulate the band gaps of the $W_{1-x}Mo_xO_3$ materials by changing the Mo/W ratio [2]. They successfully prepared a series of $W_{1-x}Mo_xO_3$ $0.33H_2O$ micro/nanostructures with controlled stoichiometry (x = 0, 0.25, 0.50, 0.75). They stated that the increase of the Mo content, the band gap of $W_{1-x}Mo_xO_3$ $0.33H_2O$ narrowed from 3.25 to 2.77 eV. In this present work we synthetized a series of $W_{1-x}Mo_xO_3$ $0.33H_2O$ nano/microstructures similar to Zhou et al. from other precursors such as ammonium heptamolybdate and ammonium metatungstate instead of metal powders. We used 2.2M HNO_3 to acidify the solutions instead of forming the peroxopolytungstic and molybdic acid solutions. Our investigation

objective was to study their enhanced band gaps as a function of the Mo content and its capability of hydrogen production.

2. Experimental

For a usual synthesis, y mmol (y = 0, 2.5, 5.0, 7.5, and 10.0) of Ammonium heptamolybdate tetrahydrate and (10 - y) mmol of Ammonium metatungstate hydrate were dissolved in a mixture of 21 mL of H_2O, 9 mL of 30 wt.% H_2O_2 , and 3 mL of 2.2M HNO_3. The solution was then transferred into a Teflon vial then placed in a stainless-steel autoclave and, sealed, and hydrothermally treated at 180°C for 24 h. The solid solutions were collected by centrifugation, washed with Deionized water 3 times, and dried at room temperature. The resultant products with y = 0, 2.5, 5.0, 7.5, and 10.0 were designated as WH1 (WO_3 $0.33H_2O$), WM25 ($W_{0.75}Mo_{0.25}O_3$ $0.33H_2O$), WM50 ($W_{0.50}Mo_{0.50}O_3$ 0.33H2O), WM75 ($W_{0.25}$ $Mo_{0.75}O_3$ $0.33H_2O$) and MH1 (MoO_3 $0.55H_2O$), respectively.

X-ray diffraction (XRD) patterns were recorded on a Philips X'Pert MPD X-ray Diffractometer with Cu KR radiation (ƛ = 1.54056 Å) at 40 kV and a current of 30 mA. Scanning electron microscopy (SEM) images were obtained on a cold field emission JEOL JSM-7401F microscope operated at 5 and 17 kV. An energy-dispersive X-ray spectroscopy (EDS) facility (Oxford INCA X-Sight) attached to the SEM was employed to analyze the chemical composition. UV-vis diffusive reflectance spectra (DRS) were obtained on a Lambda 9 UV-vis spectrometer. The Brunauer-Emmett-Teller (BET) surface areas were measured on a nitrogen adsorption apparatus (Quadrasorb SI, Quantachrome). The samples were degassed at 150-250 C for 12 h before the measurement. All ab-initio calculations were performed using the Quantum Espresso code in the framework of density functional theory (DFT). Due to the known band gap sub-estimation in DFT treatments (by the presence of "d" orbitals in W and Mo) DFT+U method was employed. The models for calculating WH1 and MH1 oxides were to reduce the unit cells from conventional to primitive, while the bimetallic solutions (WM25, WM50 and WM75) were calculated by means of 2x2x1 supercells. In all systems, the hydrated unit cell were employed (to XRD pattern fitting and to DFT calculations), however in both theoretical approach the H atoms are excluded. Hydrogen production was monitored using a gas chromatography Perkin Elmer, Clarus 500, a batch quartz photoreactor and a 250 W mercury lamp.

3. Results and discussion.

For WH1 the indexing corresponds to orthorhombic crystal, space group Aba2 and lattice parameters a = 7.323Å, b=7.690Å, c=12.772Å (calculated from ICSD using POWD- 12++ 228, 695 (1997)). For Mo fraction x = 0:25; 0:50, and 0:75 the space group was maintained, indicating that W in WO3 0.33H2O can be substituted up to 75% by Mo. According to the references [3,4] the appearance of new diffraction peaks in this case is due to the reduced symmetry from an F-centered orthorhombic cell for WO_3 $0.33H_2O$ to a C-centered orthorhombic cell for $W_{0.25}$ $Mo_{0.75}O_3$ $0.33H_2O$ caused by increased distortions induced by Mo substitution. For MH1 (x = 1.00), the XRD pattern can be assigned to hexagonal MoO_3 $0.55H_2O$

(Calculated from ICSD using POWD- 12++ 228, 695 (1997), space group P63/m, lattice parameters a= 1.0584 nm, b = 1.0584 nm, c = 0.3727 nm). All XRD patterns are included in figure 1.

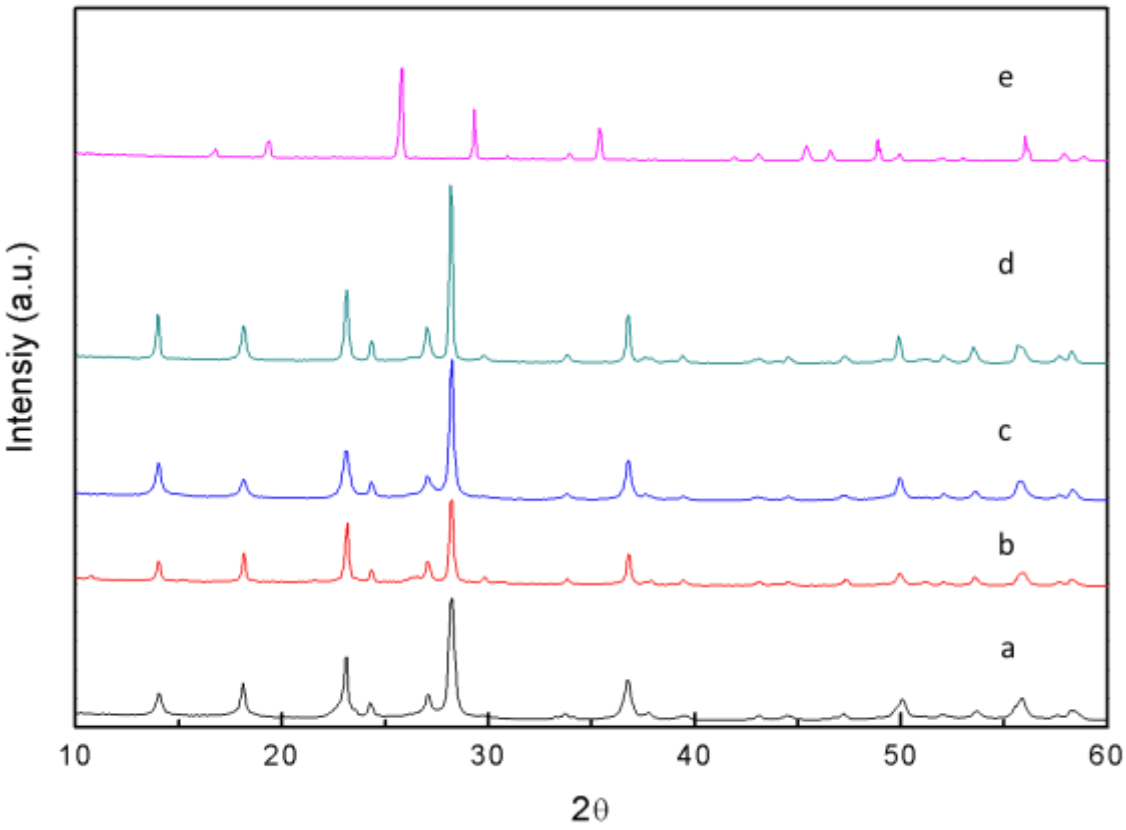

Fig 1. XRD patterns of (a) WH1, (b) WM25, (c) WM50, (d) WM75, and (e) MH1

Table 1. Theoretical and Experimental Mo Content, BET Surface Area and Band Gap

Sample	$X_{theoritical}$[1]	X_{EDS}[2]	S_{BET}[3](m^2/g)	E_g[4] (eV)	Size particle/stddev (nm)
WH1	0	0	68.2	2.62	73 ± 35
WM25	25	21	46.0	2.5	337 ± 223
WM50	50	37	40.1	2.45	103 ± 65
WM75	75	55	15.0	2.10	163 ± 57
MH1	100	100	1.0	2.37	29000 ± 15000

[1]Theoretical Mo content, [2]Mo content determined from EDS, [3]BET surface area, [4]Band gap

There are two major factors that influence the BET surface areas of the products, that is, the particle size and the Mo content. WH1 compound shows the largest BET surface area of 68.50 m^2/g due to the high W content. For the $W_{1-x}Mo_xO_3$ $0.33H_2O$ solid solutions, the particles size (the size of the primary particles) play a more important role. With the increase of the Mo content from 0 to 0.75, the BET surface area of the products decreases from 68.50 to 15 m^2/g, which can be attributed to the increase of the primary particle size deduced from the sharpening of the diffraction peaks shown in the XRD patterns.

Figure 2 represents the SEM images of the solid solutions. For WH1 (2a), WM25 (2b), WM50 (2c) and WM75 (2d), the products are mainly composed of nanometer sized flakes (200 nm in size). We can observe micro irregular particles for MH1 (2e) with widths and lengths of approximately 29000±15000 nm. Measurements values can be found in Table 1

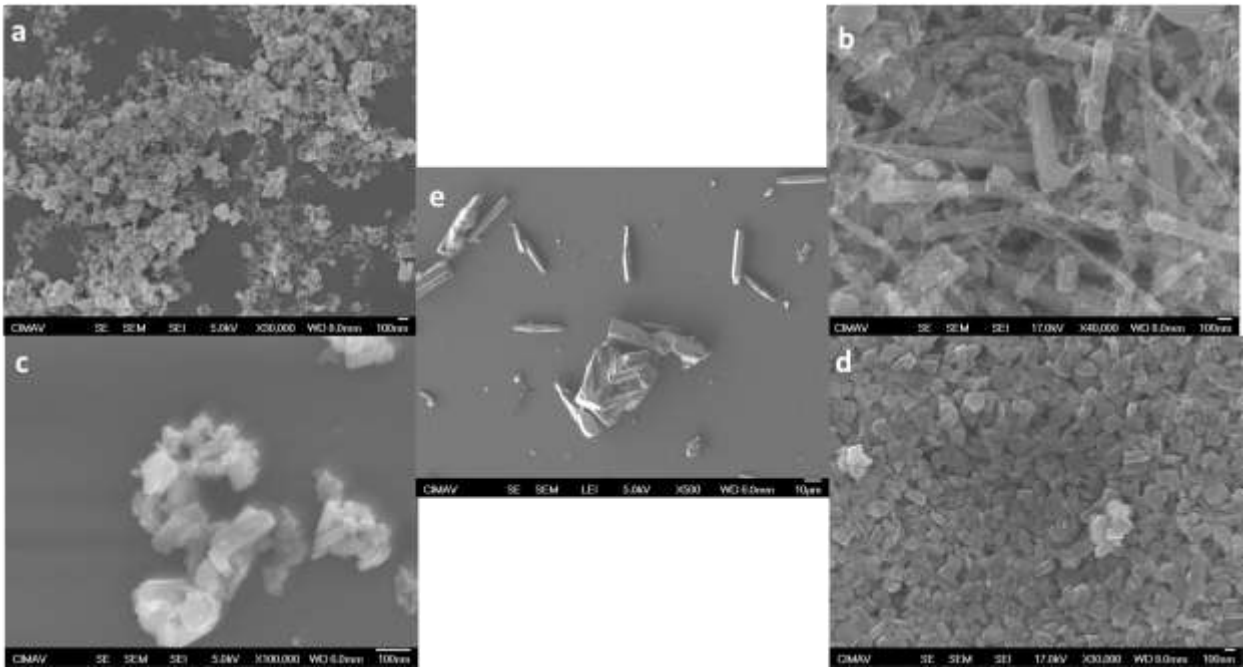

Fig 2. SEM images of (a) WH1, (b) WM25, (c) WM50, (d) WM75, and (e) MH1

From the absorption spectra of the samples, it is under stood that substitution shifts the absorption edge of $W_{1-x}Mo_xO_3$ $0.33H_2O$ from the UV to visible region (figure 3a). Now, we can determine the effective reduction in the band gap (BG) of these solid solutions due to the incorporation of Mo. Figure 3b shows the band gap of all samples. The line drawn on the linear part of [F(R)h]1/2 vs. hcurve at [F(R)h]1/2 = 0 gives the band gap. In pure WO_3, the electronic transition occurs directly from VB to CB. For the W/Mo samples, the results are rather similar to that of WO_3 $0.33H_2O$ except that they show more absorption in the visible range (~440 nm). With the introduction of 25% of Mo, a significant shift can be observed

(compared against WO_3 $0.33H_2O$), indicating a narrowing of the band gap. With even more Mo fraction, shifts can be observed. For x = 0.25, 0.50, and 0.75, the band gaps of the solid solutions are 2.50, 2.45, and 2.10 eV, respectively. The band gap of MH1, which is 2.30 eV, does not follow the trend of the $W_{1-x}Mo_xO_3$ $0.33H_2O$ solid solutions due to its structural difference. The DRS results clearly demonstrate the importance of structure (crystalline phase) in studying the composition-property relationship of the binary $W_{1-x}Mo_xO_3$ materials. We believe that the narrowing of the BG is because of the additional fraction of Mo as Zhou et al. stated: "The increased M^{5+} fraction and thus enhanced intervalency-transition are responsible for the narrowing of the band gap".

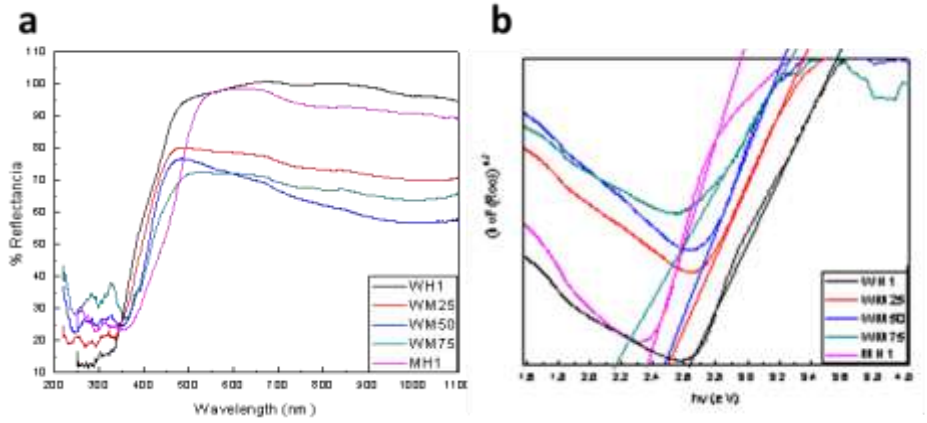

Fig 3. Diffuse reflectance and band gap determination. (a) Diffuse reflectance (%R) spectra of solid solutions (b) Determination of band gap of each samples by drawing a line at [F(R)h]1/2 = 0

DFT calculations resulted in decrease of the electronic gap in function of Mo addition, going from 0.491, 0.435, 0.433 and 0.418 eV to WH1, WM25, WM50 and WM75 respectively. However metallic character was obtained in MH1 compound; in disagree to experimental measured value. The gap trend was also investigated by incorporating the Hubbard correction, optimizing the on-site Coulomb value in WH1 to U = 6 eV. This U value was extended to all other compositions, to take an approach that is independent of the amount of added Mo, the potential was applied over "d" orbital of oxygen atoms. The band structure showed in Figure 4 correspond to our results of DFT+U, which had the same gap trend; i.e. the gap decrease function of the Mo amount, obtaining 2.63eV for WH1, 2.26eV for WM25, 2.04eV for WM50 and 1.98eV for WM75 and indirect gaps. The gap reduction (and the enhanced efficiency in photocatalysis) by adding Mo is because of the extra bands below the conduction bands. Our model correctly captures the current trend WH1 to WM75. Regarding MH1 structure, equal to DFT result, it was not possible to obtain semiconductor character. The clear relationship between band structures of the hydrated compound MH1 and its unhydrated analogy Mo_2O_3, which presents electronic gap (not shown), suggest that the measured gap could result from the combined presence of molybdenum oxide created by

O vacancies. Different MH1 models with O vacancies were tested, despite the metallic character was not modified. In our employed models, it was not possible to investigate the importance of taking into account H atoms (thus dispersive forces) and its effect on the electronic gap, however will be presented in a future work.

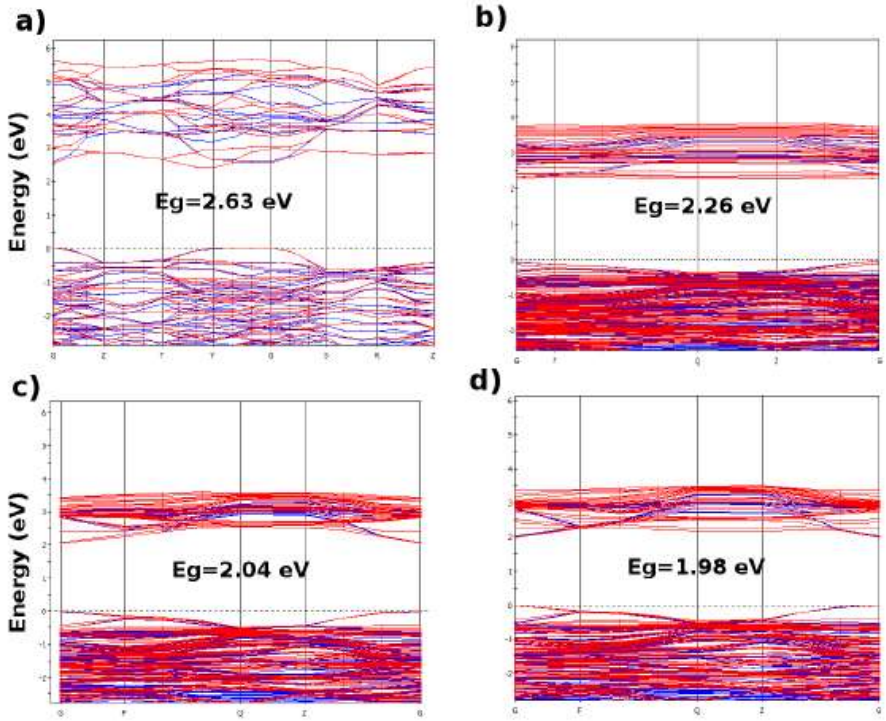

Fig 4. Band structures obtained from the conventional unit cell: a)WH1, and from primitive unit cells: b)WM25, c)WM50 and d)WM75. The U value corresponds to 6 eV.

The photocatalyc activity evaluation of the compounds was monitored through the evolution of the hydrogen produced by the dissociation reaction of the water molecule via photocatalysis. Results are shown in table 2. There was very little production of hydrogen and we believe it is because of the nature of WO_3 itself. We found studies that have shown that WO_3 is a visible light responsive photocatalyst with a relatively narrow band-gap energy (2.4–2.8 eV) and a VB potential similar to that of TiO_2 [5]. Therefore, the oxidizing power of holes in the VB of WO_3 and TiO_2 are considered to be almost the same. However, pure WO_3 is not an efficient photocatalyst because of its low CB level, which limits the photocatalyst's ability to react with electron acceptors such as oxygen [6]. The low CB level also increases the recombination of photo-generated electron–hole pairs leading to lower photocatalytic activity.

Table 2. Photocatalytic hydrogen production

Compound	μmoles H_2/g_{cat}
WH1	10
WM25	11
WM50	15
WM75	20
MH1	5

4. Summary and perspectives

We have synthesized a series of $W_{1-x}Mo_xO_3$ $0.33H_2O$ solid solutions with controlled stoichiometry (x = 0, 0.25, 0.50, 0.75). The lattice of WH1 (WO_3 $0.33H_2O$) can be substituted with up to 75% Mo without structural alteration. When we increase the content of Mo, the band gap of the $W_{1-x}Mo_xO_3$ $0.33H_2O$ structure narrowed from 2.62 to 2.10 eV. We believe that the enhanced intervalency-transitions, pressure, temperature and pH are responsible for the narrowing of the band gap and increasing the superficial area. DFT+U calculations confirmed our experimental data and showed that gap narrow was due to added bands below conductions level of the original WH1 compound. Hydrogen production was reached after 4h of irradiation for each compound. Compound WM75 had the maximum amount produced that was 20 μmoles H_2/g_{cat}. We think that the properties of these enhanced compounds make them suitable for applications like photocatalysis or gas sensing.

Acknowledgments

The authors are thankful with Centro Nacional de Supercomputo (CNS) del Instituto Potosino de Investigacion Cientifica y Tecnologica (IPICyT) for computational resources, with CIMAV NANOTECH and Rodrigo Dominguez for provided support. JCC is supported by CONACYT scholarships 290674 and 290604.

References

[1] Ni M, Leung MKH, Sumathy K, Leung DYC. Water electrolysis—a bridge between renewable resources and hydrogen. Proceedings of the International Hydrogen Energy forum, vol. 1, 25–28 May 2004, Beijing, PRC. p. 475–480.
[2] L. Zhou, J. Zhu, M. Yu, X. Huang, Z. Li, Y. Wang, and C. Yu, The Journal of Physical Chemistry C 114, 20947 (2010).
[3] F. Harb, B. Gerand, and M. Figlarz, C. R. Acad. Sci. Paris 303, 789 (1986).
[4] H. F., Solid State Ionics 32-3, 84 (1989).
[5] M. Miyauchi, M. Shibuya, Z. G. Zhao and Z. Liu, J. Phys. Chem. C, 2009, 113, 10642.
[6] M. Miyauchi, Phys. Chem. Chem. Phys., 2008, 10, 6258.